

# We are IntechOpen, the world's leading publisher of Open Access books Built by scientists, for scientists

6,900

Open access books available

186,000

International authors and editors

200M

Downloads

Our authors are among the

154

Countries delivered to

TOP 1%

most cited scientists

12.2%

Contributors from top 500 universities



WEB OF SCIENCE™

Selection of our books indexed in the Book Citation Index  
in Web of Science™ Core Collection (BKCI)

Interested in publishing with us?  
Contact [book.department@intechopen.com](mailto:book.department@intechopen.com)

Numbers displayed above are based on latest data collected.  
For more information visit [www.intechopen.com](http://www.intechopen.com)



# Wind Power Integration: Network Issues

Sobhy Mohamed Abdelkader

<sup>1</sup>Queens University Belfast

<sup>2</sup>Mansoura University

<sup>1</sup>United Kingdom

<sup>2</sup>Egypt

## 1. Introduction

Rise of energy prices and the growing concern about global warming have exerted big pressure on the use of fossil fuels to reduce emissions especially CO<sub>2</sub>. Instability in some of the major oil producing countries may affect the supplies and price of oil. On the other hand the growing need for energy consumption cannot be stopped or even limited as it is directly related to the rate of development and the standard of living. Renewable energy systems offer a solution to these conflicting issues by providing a clean energy that can supply a reasonable share of the total energy requirement without contributing to air pollution. With the 20% target of the total energy consumption to be supplied by renewable energies by 2020, and the high potential of wind energy in most European countries, wind energy systems are being installed and the penetration levels of wind energy into the electrical power systems are increasing at high rates.

Concerns about integrating wind power at high penetration levels arise from the fact that the conventional network is well suited for large synchronous generators with firm capacity and fully controlled output; this network is faced with a large number of wind farms utilizing either Induction Generators (IGs) or Doubly Fed IGs (DFIGs) with small capacity spread over different voltage levels. IGs and DFIGs have no inherent voltage control capability; it is rather reactive power loads adding to the system reactive power burden and voltage control problems. Moreover, wind farms are usually installed at remote areas where strong connections to the network is are not available. The capability of the existing network to accommodate the power generated from wind becomes an important issue to investigate. The unusual power flow patterns due the injection of power at nodes at the load ends of the network require reviewing the protection system settings and may need new protection schemes based on new rules to suite the new situation.

The focus of this chapter will be on the voltage stability problem and the network capability to accommodate power from the wind. As the chapter is aimed to be a teaching tool, analysis is presented in a graphical manner using a simple two bus system.

## 2. Voltage stability

Voltage stability analysis methods can be categorized into either steady state or dynamic methods. The steady state methods make use of a static model such as power flow model or a linear model for the system dynamics about the steady state operating point. On the other

hand dynamic methods use a model characterized by nonlinear differential and algebraic equations which is solved by time domain simulations. Dynamic methods provide accurate replication of the actual events and their chronology leading to voltage instability; it is however very consuming in terms of computation time and the time required for analysis of the results. Moreover, it does not easily provide sensitivity information or the degree of stability. Static methods with their much less computing time requirements together with its ability to provide sensitivity information and the degree of stability are being widely used to provide much insight to voltage stability. The degree of stability is determined either by the calculation of either a physical margin (load margin, reactive power margin, etc.) or a measure related to the distance to collapse.

Most of the tests for voltage stability assessments consider the steady state stability of the power system and do not differentiate between voltage and angle stability. Only few methods such as [7] use separate tests for voltage stability and angle stability. As we are concerned with voltage stability, it is more suitable to work on the voltage plane and not on the parameter space to detect genuine voltage stability problems. For this purpose, a graphical interpretation of the problem is developed based on representation of the parameters of each load bus in the complex voltage plane. Basics of the graphical approach for the assessment of voltage stability in power systems are presented using a simple two bus power system. Despite its simplicity, the two bus system helps a lot in clarifying the issue because it can be handled easily by analytical methods. This helps in the acquisition of the required knowledge and concepts which can then be generalized to real power systems of any size. It is also straightforward to find a two node equivalent to a multi node power system at any of its ports. This fact makes most of the conclusions drawn from the two node system valid for a general power system.

With wind power integrated into the electrical power system at high penetration levels, the situation becomes a bit different. Power is being injected at PQ nodes. In addition to the changed power flow patterns, the characteristics of the PQ nodes, at which wind generators are connected, also changed. Wind as a stochastic source has also introduced a degree of uncertainty to the system generation.

### 2.1 Graphical interpretation of voltage stability limit

As mentioned above all the analysis in this chapter will be carried out for a two bus system. The system, as shown in Fig.1, has only one line of series impedance  $Z$  and no shunt admittance. The effect of the line charging can be taken into consideration by using the Thevenin's equivalent of the system at the load bus. One of the two buses is considered a slack bus with constant voltage  $E$  while the other one is the load bus at which voltage stability is to be studied.

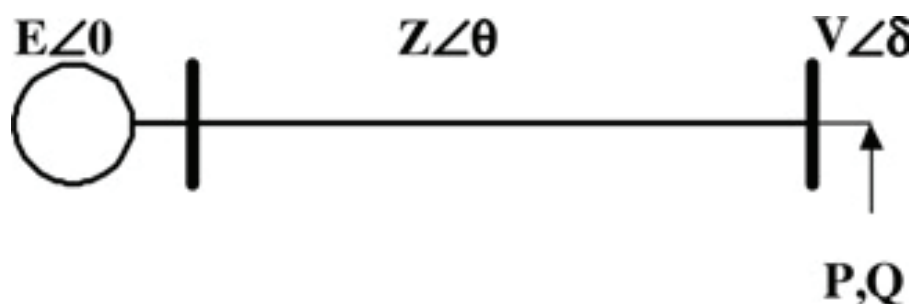


Fig. 1. Two bus system

Throughout the analysis the following symbols and conventions are adopted.

Z: impedance magnitude of the line

$\theta$ : impedance angle of the line

R: the line resistance

X: the line reactance

V: voltage magnitude at the load bus

$\delta$ : voltage angle at the load bus

P: active power injected at the load point

Q: the reactive power injected at the load.

**V, E** and any other bold variable means that it is a phasor variable

For the system of Fig.1, active power and reactive power balance equations can be written in the following forms:

$$-P = \frac{V^2}{Z} \cos(\theta) - \frac{EV}{Z} \cos(\theta + \delta) \quad (1)$$

$$-Q = \frac{V^2}{Z} \sin(\theta) - \frac{EV}{Z} \sin(\theta + \delta) \quad (2)$$

Eqns. (1) and (2) represent constraints on the load bus voltage and must be satisfied simultaneously. All the points in the complex voltage plane that satisfy the two constraints are possible solutions for the load bus voltage. If the system fails to satisfy these constraints simultaneously, this means that the stability limit has been exceeded and no solution will exist. These constraints will be plotted in the complex voltage plane to find the possible solutions for the voltage and also to define the voltage stability limit. Steady state analyses of power system assume constant active power, P, and constant reactive power, Q, at all load nodes and for generators reaching any of their reactive power limits. This assumption works very nicely for power flow studies and studies based on snap shot analysis. However, if the purpose is to find out the stability limit, such assumption may be misleading. In case of large wind farm connected at a relatively weak point, it will not be accurate to consider the constant P Q model. In the following sections the effect of P and Q characteristics on voltage stability limit is illustrated. Three different characteristics are examined; constant P and constant Q, quadratic voltage dependence, and induction motor/generator.

### 2.1.1 Constant PQ load model

Assuming a constant active and reactive power, which is the common model for PQ nodes in power flow studies and substituting for  $V^2$  by  $(V \cos(\theta + \delta))^2 + (V \sin(\theta + \delta))^2$ , Eq. (1) can be arranged and expressed as follows.

$$\left( V \cos(\theta + \delta) - \frac{E}{2 \cos(\theta)} \right)^2 + (V \sin(\theta + \delta))^2 = \left( \frac{E}{2 \cos(\theta)} \right)^2 - \frac{PZ}{\cos(\theta)} \quad (3)$$

Equation represents a circle in the complex voltage plane. Using the rotated axes  $V \cos(\theta + \delta)$  and  $V \sin(\theta + \delta)$  rather than  $\text{real}(V)$  and  $\text{Imaginary}(V)$  makes constructing this circle easier. On the new axes, centre of the circle is located at  $(0.5E / \cos(\theta), 0)$  and its radius,

$$r_p = \sqrt{E^2 / 4 + RP / \cos(\theta)}.$$

This circle, will be referred to as p-circle, defines the locus for constant load power in the complex voltage plane and all the points on it satisfy the active power constraint. Similarly, the reactive power balance, Eq. (2), can be rearranged and written as below.

$$(V \cos(\theta + \delta))^2 + \left( V \sin(\theta + \delta) - \frac{E}{2c \sin(\theta)} \right)^2 = \left( \frac{E}{2 \sin(\theta)} \right)^2 - \frac{QZ}{\sin(\theta)} \quad (4)$$

Again, Eq.(4) represents a circle in the complex voltage plane. All points on this circle satisfy the reactive power balance constraint and it will be referred to as the q-circle. On the same axes as in the case of p-circle, centre of the q-circle is located at  $(0, 0.5E/\sin(\theta))$  and its radius

$$r_q = \sqrt{E^2 / 4 + QX / \sin(\theta)}.$$

Fig.2. shows the complex voltage plane with circles for different values of P and Q. The values used to produce this figure are:  $E=1$  pu,  $Z=0.7$  pu and  $\theta=60^\circ$ . In this figure,  $P_0=0$ ,  $P_1=0.3$ ,  $P_2=0.48$ ,  $Q_0=0$  and  $Q_1=0.23$  (all in pu). The following points can be observed from the figure:

1. Centre locations of the two circles, CP and CQ, are determined by E, Z, and  $\theta$  only. This means that the distance between the two centres remains constant as long as there is no change in E or the line impedance whatever the values of P and Q are.
2. Both of  $r_p$  and  $r_q$  are load dependant. As the load (P and/or Q) gets larger,  $r_p$  and/or  $r_q$  gets smaller. This is clear on Fig. 2 where  $r_{p0} > r_{p1} > r_{p2}$  &  $r_{q0} > r_{q1}$ .
3. As long as  $r_p+r_q$  is greater than the distance between the two centres, the two circles intersect each other in two points and hence there will be two possible voltage solutions for the load bus. The voltage solution with higher magnitude will be called the higher voltage,  $V_H$ , while the other will be called the lower voltage,  $V_L$ .
4. At light loads  $r_p+r_q$  is much greater than the distance between the centres, this causes a large difference between the points of intersection (the voltage solutions). This difference gets smaller as the load increases due to the reduction in  $r_p+r_q$ .
5. If the load is increased until  $r_p+r_q$  becomes just equal to the distance between the centres, the two solutions coincide with each other and there will be only one solution. Any further increase in either P or Q will cause even this single solution to cease to exist.
6. The circles P0 and Q0 intersect at  $V=1=E$ , and at  $V=0$ . These are the two possible solutions at no load. Increasing P to P1 while keeping Q at 0, the new voltage solutions are those defined by the two arrows. When Q increases to Q1, the two circles P1 and Q1 are tangential and the voltage solutions coalesce into one solution. Any further increase in either P or Q will cause this one solution to disappear. The circles P2 and Q0 are tangential, having one voltage solution, revealing that the loading condition (P2,Q0) is a voltage stability limit. As the figure shows, as the system approaches the stability limit the voltage solutions become closer until they coalesce in one solution. The end point of the voltage vector at the stability limit always lies on the line  $V \cdot \cos(\delta) = 0.5 \cdot E$ . Each point on this line defines a voltage stability limit for a different combination of P and Q. It is easy to prove the singularity of the load flow Jacobian at each point of this line. Each other known criterion for voltage the stability limit, such as maximum Q, maximum P, refers to a subset of the conditions defined by this line.

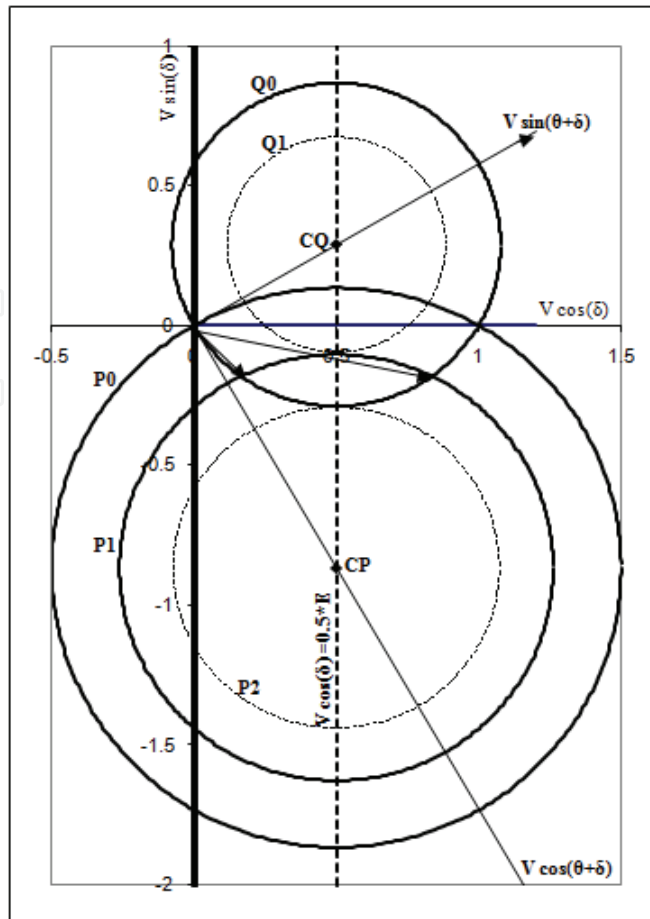


Fig. 2. Loci for active and reactive power balance constraints in the complex voltage plane

### 2.1.2 Constant impedance load

If the load is considered to have constant impedance, then both  $P$  and  $Q$  can be expressed as functions of voltage as follows:

$$P = G.V^2 \quad (5)$$

$$Q = B.V^2 \quad (6)$$

Substituting for  $P$  from (5) into (1) the active power equation can be arranged in the following form:

$$V = \frac{E}{G.Z + \cos(\theta)} \cdot \cos(\delta + \theta) \quad (7)$$

Eq.(7) represents a circle in the complex voltage plane with its centre lying on the  $V \cos(\theta + \delta)$  axis at  $V \cos(\theta + \delta) = 0.5 E / (G.Z + \cos(\theta))$  and its radius equal to  $0.5 E / (G.Z + \cos(\theta))$ . Similarly the  $Q$  equation can be re-written as:

$$V = \frac{E}{B.Z + \sin(\theta)} \cdot \sin(\delta + \theta) \quad (8)$$

which again is a circle in the complex voltage plane with its centre lying on the  $V \sin(\theta+\delta)$  axis at  $V \sin(\theta+\delta) = 0.5 E/(BZ+\sin(\theta))$  and its radius equal to  $0.5 E/(BZ+\sin(\theta))$ . Fig. 3 shows these two circles on the complex voltage plane. Inspection of the graph and the circle parameters leads to the following observations:

1. The locations of the centres of the circles are load dependant and so are the radii.
2. The two circles always have two intersection points one of which is  $V= 0.0$ . The other one depends on the load impedance. So, there is only one feasible solution. However, this solution always exists as long as the load impedance is greater than zero.
3. The nonzero voltage magnitude can be calculated from (7) and (8) as:

$$V = \frac{E}{\sqrt{1 + Z^2(G^2 + B^2) + 2BZ \sin(\theta) + 2GZ \cos(\theta)}} \quad (9)$$

It is easy to find out that this voltage decreases as  $G$  and/or  $B$  increases. This means that this voltage solution is always stable. So, for constant impedance load, there is only one possible solution and it is stable for the whole range of load impedance.

4. Active and reactive powers can be derived by substituting for  $V$  from (9) into (5) and (6) respectively yielding:

$$P = \frac{GE^2}{1 + Z^2(G^2 + B^2) + 2BZ \sin(\theta) + 2GZ \cos(\theta)} \quad (10)$$

$$Q = \frac{BE^2}{1 + Z^2(G^2 + B^2) + 2BZ \sin(\theta) + 2GZ \cos(\theta)} \quad (11)$$

But, in all cases the voltage is stable and the voltage of a system with such load can not collapse like in the case of constant power load.

5. The condition for maximum power transfer to the load bus can be derived by equating the determinant of the Jacobian matrix of  $P$  and  $Q$  w.r.t  $G$  and  $B$  to zero. This can be found to be:

$$G^2 + B^2 = \frac{1}{Z^2} \quad (12)$$

All of the points satisfying this condition are lying on the border line defined in the case of constant power load ( $V \cos(\theta+\delta) = 0.5 E$ ). However, in this case this line is not the border between stability and instability area, but it is the border between two areas with different sensitivities for load power to changes in  $G$  and  $B$ . In the area to the right hand side, load has positive sensitivity to changes in  $G$  and  $B$ , whereas in the area to the left hand side if  $G$  and/or  $B$  is increased beyond this limit, the load power will decrease, but in the two areas voltage always decreases as  $G$  and/or  $B$  increases and vice versa.

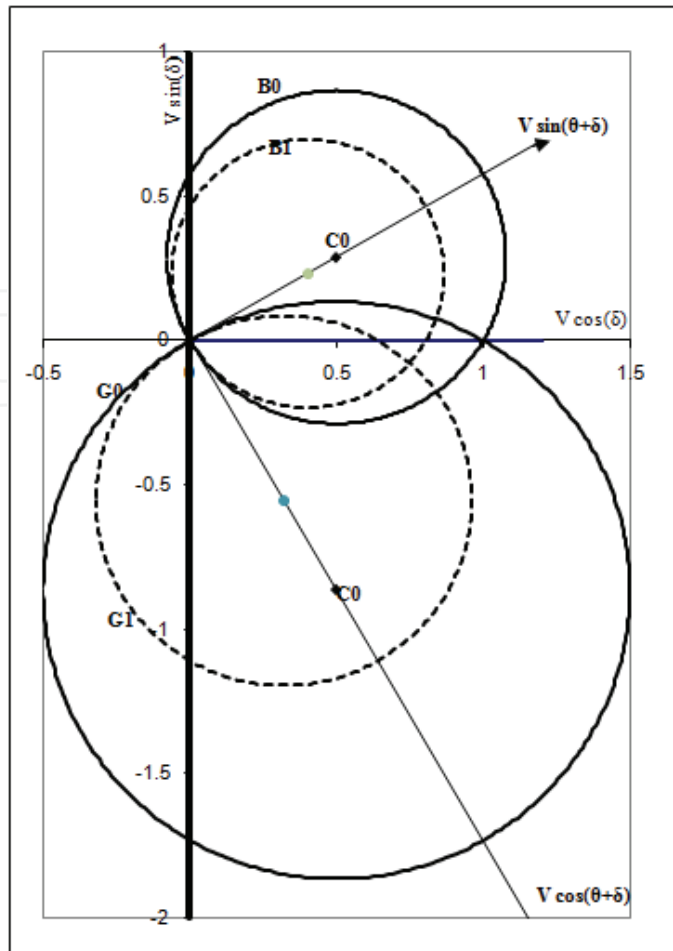


Fig. 3. Loci for constant load admittance parameters in the complex voltage plan

**2.1.3 Constant current load**

In this case, both P and Q are proportional to the load voltage magnitude i.e;

$$P = \alpha.V \tag{13}$$

$$Q = \beta.V \tag{14}$$

With the load voltage taken reference, the load current, I, will be:

$$I = \alpha - j\beta = \sqrt{\alpha^2 + \beta^2} \angle -\tan^{-1}(\beta / \alpha) \tag{15}$$

As seen from (15), the current magnitude is constant while its direction is dependent on the voltage angle. So, the voltage drop on the line will have a constant defined magnitude while its angle is unknown until the voltage direction is determined. This can be represented in the voltage plane as a circle with its radius equal to  $I.Z$  and its centre located at the end of the E vector which is on the real axis.

Since  $\alpha$  and  $\beta$  are constants, then the load power factor is also constant. The locus for a constant power factor in the voltage plane can be found (by dividing (1) by (2), equating the result with  $\tan(\varphi)$ , expanding  $\cos(\theta+\delta)$  &  $\sin(\theta+\delta)$  terms, and rearranging) to be a circle with its equation is:

$$\left( V \cos(\delta) - \frac{E}{2} \right)^2 + \left( V \sin(\delta) - \frac{E}{2} \tan\left(\frac{\pi}{2} - \theta + \phi\right) \right)^2 = \left( \frac{E}{2 \cos\left(\frac{\pi}{2} - \theta + \phi\right)} \right)^2 \quad (16)$$

This circle can be constructed in the voltage plane as follows:

- The centre is defined by the intersection of the line making an angle =  $\arctan (b/a)$  with the  $V \sin (\theta+\delta)$  axis (counter clockwise for lagging power factor and clockwise for leading power factor) and the line  $V \cos (\delta)=0.5 E$ .
- The radius is the distance between the centre and the origin.

Fig (4) shows these circles on the voltage plane for different values of load current, and different power factors. There are always two points of intersection. However, one of these points corresponds to a load condition while the other to a power injection i.e. generation. So, for load of constant current behaviour, there is always one voltage solution and this solution is totally stable according to the criterion stated before. The limiting factor in this case will not voltage stability, it would rather be the thermal limit of the lines or the voltage regulation.

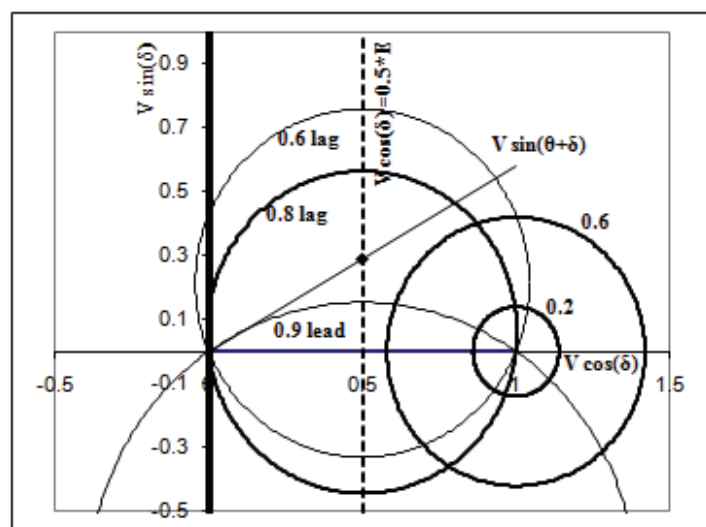


Fig. 4. Constant current and constant power factor circles in the complex voltage plane

For further comparison between the three type of loads, Fig. 5.a shows the voltage against the load parameter, i.e P for constant power load, G for constant impedance load, and  $\alpha$  for constant current load. All loads are assumed to have the same power factor of 0.8 lagging. The rest of the system parameters are  $E=1.0$  pu,  $Z=0.7$  pu, and  $\theta=60^\circ$ . This figure confirms what has been observed from Figs. 2 - 4 regarding the voltage magnitude. Fig. 5.b shows the P-V curve, which is found to be the same for all types of loads. Fig.5.c shows the maximum loading limits in the P-Q plane, and also it found to be the same for all the three cases. It is to be noted that the mapping of this limit into the voltage plane is the line which we called the border line (BL). Although the constant impedance and constant current can have a stable equilibrium point on the lower part of the P-v curve, they are not allowed to reach this part. This is because if such loads are operated in this part and it was required to shed some load, disconnecting part of these loads will increase their power demand instead of reducing it as it is desired. Also, reaching this part of the curve means that the voltage is very low.

Now, if these loads are allowed only to be operated in the upper part of the P-v curve, the stability limit will be the same for all of the three load types. Bearing in mind that the locus of the stability limit in the voltage plane is the BL defined above, therefore if the voltage solution lies on that line, the voltage stability limit is reached. This means that the voltage solution at the stability limit is determined by the intersection point of the P- locus, the Q locus and the BL. In other words, if the intersection point of the P-locus with the BL and the intersection point of the Q-locus with the border line coincide with each other, the voltage stability limit is reached.

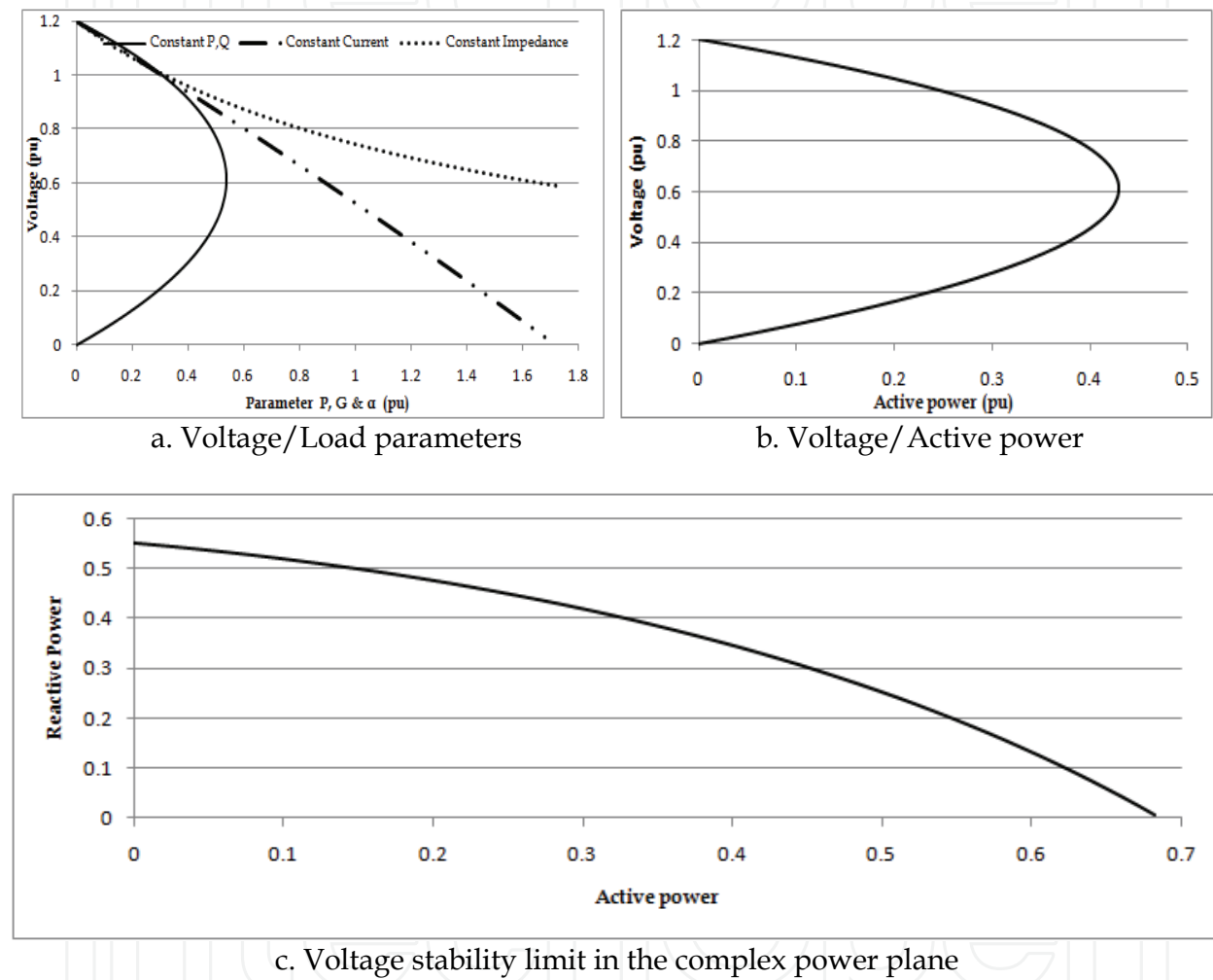


Fig. 5. Comparison of the behaviour of different types of loads regarding voltage stability

The fact that the border line between voltage stability and voltage instability region is the same, in terms of active power and reactive power, makes almost all voltage stability assessment methods use one of the features of this border line as a voltage stability measure or indicator.  $V \cos(\delta) = 0.5 E$ , which is the border line equation in the voltage plane, is one form of the indicator introduced by Kessel P. & Glavitch, H. (1986). At any point on the BL, the voltage is equal in magnitude to the impedance drop; this implies that the load impedance is equal in magnitude to the system impedance, which was used as another indicator by Abdelkader, S. (1995) and Elkateb, M. et al (1997) have presented mathematical proofs for the indicators introduced by Chebbo, A. et al (1992)., Semlym, A. et al (1991),

Tamura, Y et al (1983) and Kessel P. & Glavitch, H. (1986) are all different characteristics or features of the border line.

If a wind farm employing IGs or DFIGs is connected to the network at a node where it represents the major component of the power injected at that node, the models described above will not be suitable to represent the wind generators for assessing voltage stability. Moreover, the voltage stability limit will be different than the border line defined above. Abdelkader, S. & Fox, B. (2009) have presented a graphical presentation of the voltage stability problem in systems with large wind farms. The following section describes how voltage stability in case of large penetration levels of wind power is different than the case of constant or voltage dependant loads.

## 2.2 Voltage stability of wind generators

It is assumed here that IG is employed as a wind turbine generator. If an IG is connected at load node of the two node system, the equivalent circuit of the system will be as shown in Fig. 6.

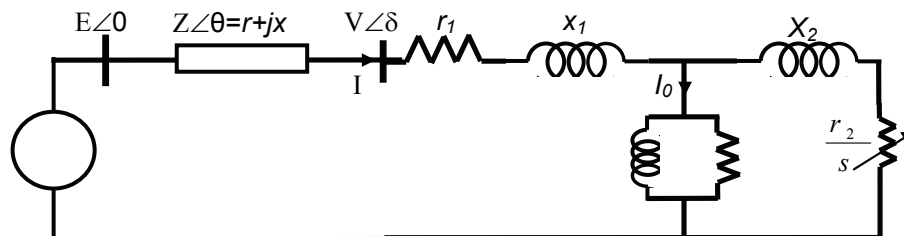


Fig. 6. Equivalent circuit of the two bus system with IG

Neglecting the no load current,  $I_0$ , the current delivered by the induction generator to the system can be calculated as

$$I = \frac{E}{(r + r_1 + \frac{r_2}{s}) + j(x + x_1 + x_2)} \quad (17)$$

Voltage at the end of the transmission line can be calculated as follows.

$$V\angle\delta = E\angle 0 - \frac{E}{(r + r_1 + \frac{r_2}{s}) + j(x + x_1 + x_2)} \cdot Z\angle\theta \quad (18)$$

With  $s$  as a parameter, the voltage vector locus in the voltage plane can be obtained through some manipulations of (18). It is found to be as follows.

$$\left( V \cos(\delta) - \left( E - \frac{E \cdot x}{2(x + x_1 + x_2)} \right) \right)^2 + \left( V \sin(\delta) - \frac{E \cdot r}{2(x + x_1 + x_2)} \right)^2 = \left( \frac{E \cdot Z}{2(x + x_1 + x_2)} \right)^2 \quad (19)$$

Equation (19) represents a circle in the complex voltage plane. The coordinates of its centre, CG, and its radius are clearly defined in (19). Fig. 7 shows the complex voltage plane with the IG circle diagram. System data are same as for Fig.2. IG data used to produce this figure are  $x_1 = x_2 = 0.2$  pu and  $r_1 = r_2 = 0.05$  pu. The figure displays the locus of the IG voltage, the

circle centered at CG, the loci for  $Q=0$  and  $P=0$ . The figure shows clearly that even with the magnetizing current neglected the IG cannot deliver any power at  $Q=0$  as the IG circle has no intersection points with  $Q=0$  except at  $P=0$ . When reactive power consumed at the point of connection increases, radius of the  $Q$  circle gets smaller and there will be two intersection points where the IG can deliver power.

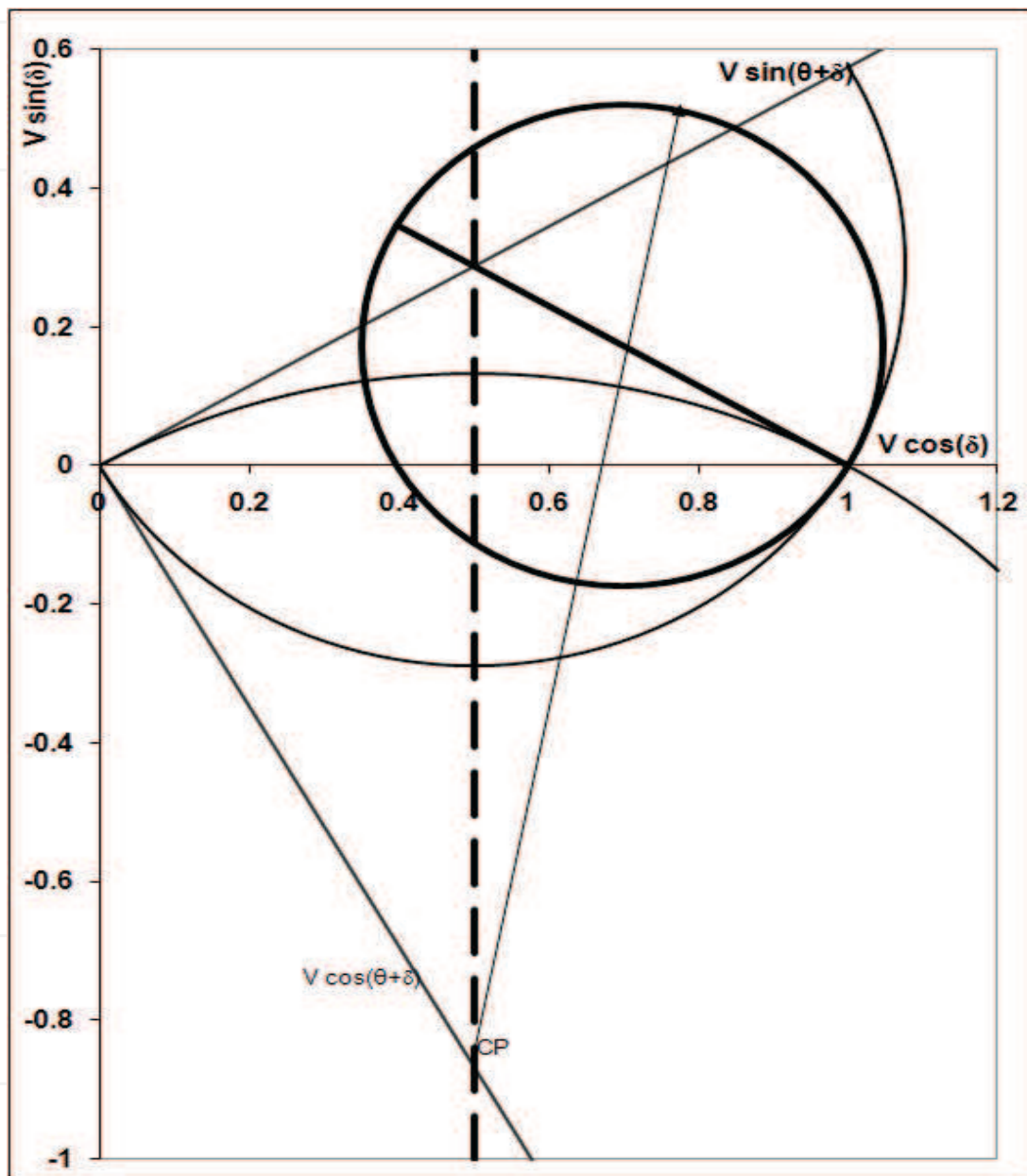


Fig. 7. Complex voltage plane for the case of IG

As the power delivered by the IG increases, the  $P$ -circle radius increases until a value is reached where the  $P$  circle becomes tangent to the IG circle at the point  $P_m$  in Fig. &. This is the maximum limit of the IG power. No equilibrium point exists if  $P$  is increased beyond this limit. The point of maximum power, or the steady state stability limit,  $P_m$ , is determined by connecting the centres of the IG and the  $P$  circles with a line and extending it until it intersects the IG circle in  $P_m$ . The most important thing to note is that the stability

limit is no longer the same for the case of constant PQ load, the dashed line on Fig. 7. Therefore, all the indicators based on the PQ load model might be misleading if used for the case of IG. In other words, voltage stability in case of a WF employing IGs is not determined by only the terminal conditions of the IG, P and Q injections, but also by the IG characteristics. It is also clear that at each active power output from the IG there is a specific value of reactive power that has to be consumed by the IG. Nothing new about that, but the new thing the graph offers is that the reactive power support required at each active power output can be determined. Moreover, other limits of voltage magnitude, maximum and minimum, as well as the thermal capacity of the line connecting the farm to the system can all be represented graphically in the complex voltage plane. This enables to determine which of these limits are approached or violated. Mapping these into the complex power plane helps fast determination of a quick local remedial action.

### 2.2.1 Application to multi node power system

To apply the graphical method to assess the voltage stability of IG, the power system is to be reduced to its Thevenin equivalent at the node where the IG is installed. A method for finding the Thevenin equivalent using multiple load flow solutions is described by Abdelkader, S & Flynn, D. (2009) and is used in this paper. Thévenin's equivalent is determined using two voltage solutions for the node of concern as well as the load at the same node. The first voltage solution is obtained from the operable power flow solution while the second is obtained from the corresponding lower voltage solution. The voltage for the operable solution is already available within data available from the EMS and hence it will be required to solve for the lower voltage solution. The Thévenin's equivalent can be estimated using the two voltage solutions as follows.

$$E_{TH} = \frac{\left| \bar{V}_H \right|^2 - \left| \bar{V}_L \right|^2}{\left| \bar{V}_H - \bar{V}_L \right|} \quad (20)$$

$$\left| Z_{TH} \right| = \frac{\left| \bar{V}_H \right| \cdot \left| \bar{V}_L \right|}{\sqrt{P^2 + Q^2}}, \quad \Theta_{TH} = \Phi - \delta_H - \delta_L \quad (21)$$

Where  $V_H$  and  $V_L$  are the complex values for the higher and lower voltages of the load node, P is the active power, Q is the reactive power,  $\theta_{TH}$  is the angle of  $Z_{TH}$ ,  $\Phi = \text{atan}(Q/P)$ , and  $\delta_H, \delta_L$  are the angles of the high- and low-voltage solutions respectively. A graph for a multi-node power system having a WF connected at one of its nodes is developed as follows.

1. An IG equivalent to the WF is to be determined. Assuming that all generators of the WF are identical, the equivalent IG rating will be  $MVA_{eq} = MVA \cdot n$ , and  $Z_{eq} = Z/n$ . MVA is the rating of one IG, n is the number of IGs in the farm, and Z stands for all impedance parameters of one IG.
2. A Thevenin equivalent is determined at the WF terminal using (20), (21).
3. The system graph with the IG in the complex voltage plane is drawn as described above.

4. The graph can be mapped into the complex power plane bearing in mind that any a point  $(x,y)$  in the voltage plane maps to a point  $(p,q)$  in the complex power plan, where  $p, q$  are related to  $x,y$  by the following equations.

$$p = \frac{x.E - (x^2 + y^2)}{Z} \cos(\theta) - \frac{E.y}{Z} \sin(\theta) \quad (22)$$

$$q = \frac{x.E - (x^2 + y^2)}{Z} \sin(\theta) + \frac{E.y}{Z} \cos(\theta) \quad (23)$$

### 2.3 Test case

The IEEE 30 bus system with the standard data is used as a test system. A WF is connected at bus 30. The DIgSilent power factory is used for power flow solution of the detailed system model with the WF installed. The WF consists of 50 IG 900 kW each. The IG is rated at 6.6 kV with  $X=0.1715581$  pu, and  $R/X=0.1$ . The magnetizing current  $I_m$  is assumed to be 0.1pu.

The higher voltage solution of bus 30 for the standard case data is  $V_H = 1.0056 \angle -12.63^\circ$  pu, and the corresponding lower voltage solution is  $V_L = 0.0782 \angle -65.65^\circ$  pu. Parameters of the Thevenin equivalent for bus 30 are  $E_{TH} = 1.0463$  pu and  $Z_{TH} = 0.7302 \angle 70.64^\circ$  pu.

Fig. 8 shows the complex voltage plane with the graphs of bus 30 and the equivalent IG. The figure also shows the voltage limits constraints,  $V_{min} = 0.95$  pu and  $V_{max} = 1.05$  pu. The thermal capacity of the line connecting the WF to bus 30 is assumed 0.6 pu and is also represented in Fig. 8. The magnetizing current of the IGs is taken into consideration as it can be noticed by shifting the IG circle along the line A-GC by  $I_m \cdot Z_{TH} / (X_{th} + X)$ ,  $X_{th} = Z_{TH} \cdot \sin(\theta)$  and  $X$  is the IG reactance.

It can be noticed that maximum power point of the IG is not the PQ voltage stability line as discussed earlier. The voltage stability limit will not  $V \cos(\delta) = 0.5 E_{TH}$  as in the case of PQ load, but it will be the max power line on Fig 8. The stable operating range of the IG is thus the part of the circle starting at point A passing through points B, C, D, E, and ending at Pm, the maximum power point.

Fig 9 shows the system loci and limits mapped to the power plane and it reveals important information. First, the range of power output from the WF extends from point A up to point Pm. The value of Pm for this case is found to be - 64.8 MW. This is verified through running the detailed power flow analysis of the system on DIgSilent software. The WF power, P, is increased until the power flow diverges. The maximum value P at which the power converges is found to be the same as that obtained from the graph. That is  $P_m = 64.7$  MW. The graphical method is also verified by running the detailed power flow solution with WF power values corresponding to points B, C, D, and E. The results were in perfect agreement with that obtained from the graph.

It is interesting to note that along A-B, the WF delivers its output with all constraints satisfied. Between B and C, the maximum voltage constraint is violated. From C to D, all constraints are satisfied again. Between B ( $P=13.7$  MW) and C ( $P=38.6$  MW), more reactive power will need to be consumed to get the voltage back below the maximum voltage limit. This can be obtained from the graph by the vertical difference between the IG line and the

maximum voltage limit line. At D, the thermal capacity of the line connecting the WF to the system is reached. From D to E, only the thermal capacity limit is violated. The graph shows that a reactive power equal to the vertical difference between the IG line and the thermal limit line will relieve the overload. This can be done as long as no other constraint is violated. So, many indications about the system state and also corrective measures can be obtained using this simple graph. Most of these are tested using the detailed power flow analysis.

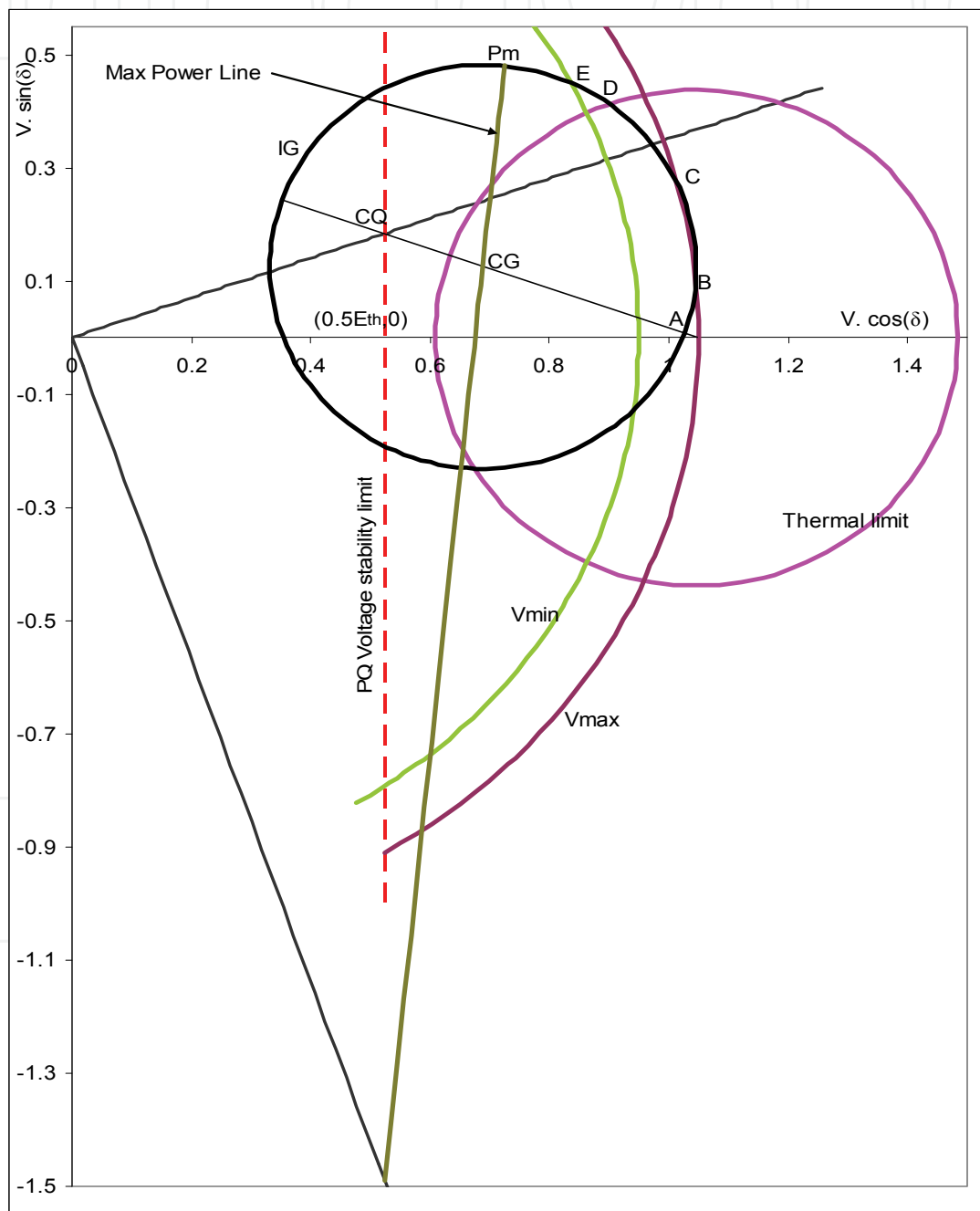


Fig. 8. Complex voltage plane for bus 30 of the IEEE 30 bus system with IG

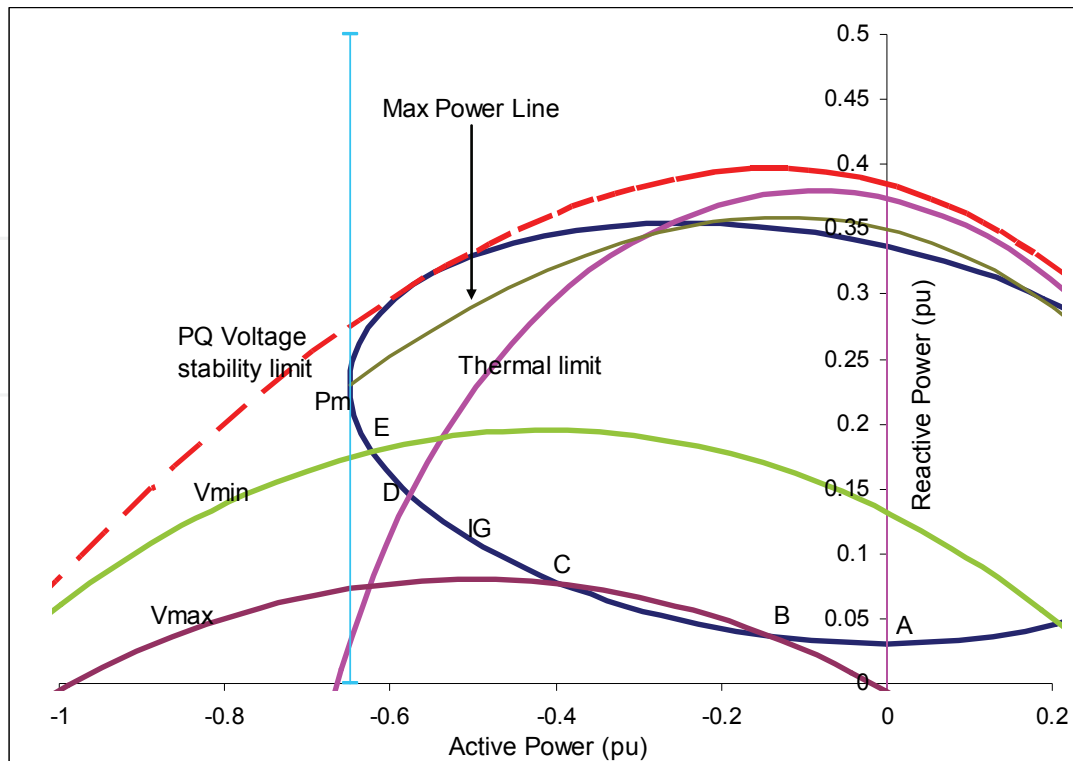


Fig. 9. Power plane graph for bus 30 of the IEEE 30 bus system with IG

### 3. Capability chart

This section presents a graphical method for determining network limits for wind power integration. For each candidate node, where a wind farm is planned, a capability chart is constructed defining the allowable domain of power injection where all operating and security constraints are satisfied. Like what has been done in sec. 2, operating and security constraints are graphically constructed in the complex voltage plane and then mapped to the complex power plane defining the allowable operating region of wind generator/farm.

#### 3.1 Graphical representation of operation and security constraints

The available generation limits both active and reactive power, thermal limits of the transmission line, upper and lower voltage limits and voltage stability limit at the node where the WF is connected are all considered. As has been done in section 2, all the analysis is carried out on the simple two bus system of Fig.1. Application to a multimode power system will be done using Thevenin equivalent in the same manner described above. The reader is advised to refer to Abdelkader, S. & Flynn D (2009) for detailed analysis and applications. In this chapter, the idea is introduced in a simple manner that makes it suitable for teaching.

##### 3.1.1 Generator power limits

The active power of the generator of the simple system of Fig. 1 can be determined as:

$$P_G = \frac{E^2}{Z} \cos(\theta) - \frac{E.V}{Z} \cos(\theta - \delta) \quad (24)$$

which can be rearranged as follows:

$$V \cdot \cos(\theta - \delta) = E \cdot \cos(\theta) - \frac{P_G \cdot Z}{E} \quad (25)$$

Eqn. 25 represents a straight line in the complex voltage plane, and although it is easy to draw such a relation on the reference ( $V \cdot \cos(\delta)$  &  $V \cdot \sin(\delta)$ ) axes, it is much easier to do so on the rotated  $V \cdot \cos(\theta - \delta)$  axis shown in Fig. 10, where a particular value of  $P_G$  correspond to a line perpendicular to this axis. Figure 2 shows the line AB representing  $P_G=0$  which is drawn from the point A( $E,0$ ) on the  $V \cdot \cos(\delta)$  axis perpendicular to the  $V \cdot \cos(\theta - \delta)$  axis. Other values of  $P_G$  can be represented by lines parallel to the line AB, but shifted by a distance representing  $(P_G \cdot Z/E)$ . The maximum  $P_G$  line is thus a line parallel to AB and shifted from it by a distance of  $(P_{Gmax} \cdot Z/E)$ , line P-P in Fig. 10. The minimum limit on  $P_G$  is also represented by the line marked  $P_{Gmin}$ .

The reactive power of the generator, given by (26), can also be rearranged in the form of (27) below.

$$Q_G = \frac{E^2}{Z} \cdot \sin(\theta) - \frac{E \cdot V}{Z} \cdot \sin(\theta - \delta) \quad (26)$$

$$V \cdot \sin(\theta - \delta) = E \cdot \sin(\theta) - \frac{Q_G \cdot Z}{E} \quad (27)$$

Similar to the case for active power, it is clear that (27) represents a straight line in the complex voltage plane. Examining the geometry of Fig. 10 confirms that the line AC perpendicular to the  $V \cdot \sin(\theta - \delta)$  axis and passing through the point A represents the zero reactive power line. The maximum reactive power line is Q-Q which is parallel to AC and shifted by  $(Q_{Gmax} \cdot Z/E)$  from AC, while the minimum reactive power limit is represented by the line marked  $Q_{Gmin}$ . Hence, the shaded area bordered by the active and reactive power constraints represents the area of feasible generator. Upper and lower active power limits of the generator are both positive, while the lower reactive power limit is assumed negative. These is common for synchronous generators. However, in this work negative lower limit for active power of the slack bus will be expected in the case of representing the equivalent of a multi node power system. Negative lower limit of active power generation means that the active power injected at the PQ node will have a capacity credit so that the scheduled conventional generation in the system is less than the total load.

### 3.1.2 Transmission line thermal limit

Thermal limit of the transmission line is defined by the maximum allowable current. Representing a constant current in the complex voltage plane is discussed in section 2.1.3 and the graphical representation is shown in Fig. 4 above.

### 3.1.3 Voltage stability limit

As discussed above, voltage stability limit in case of static loads (constant power, constant current, and constant impedance) is the line  $V \cos(\delta) = 0.5 E$  and it is drawn and marked on figs 2, 3. The voltage stability limit in case of IG is different, but in this chapter voltage stability is considered the same as for static loads. This is to keep presentation of the capability chart as simple as possible.

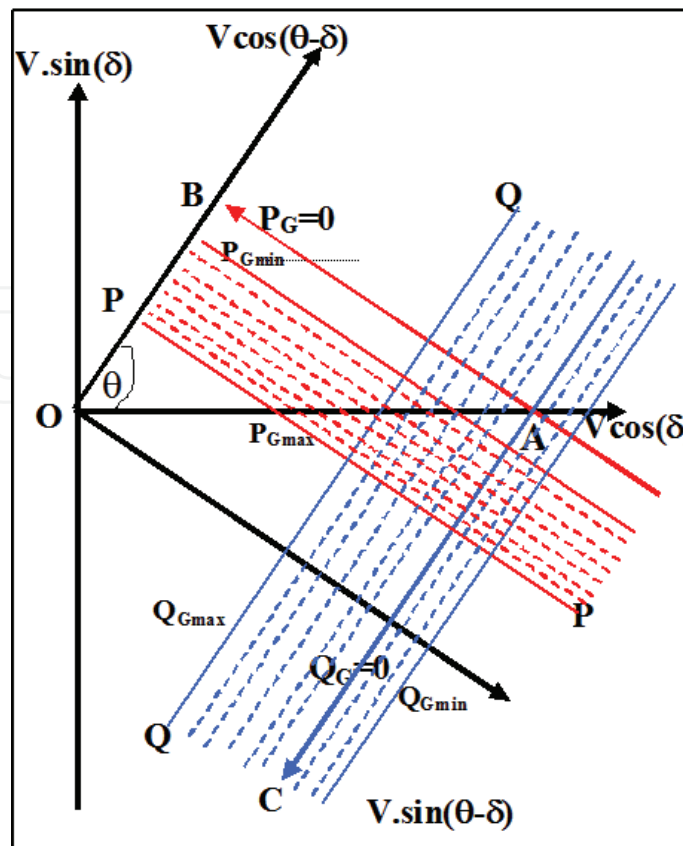


Fig. 10. Generator capability limits in the complex voltage plane of the load node

### 3.1.4 Maximum and minimum voltage limits at the WF terminals

Voltage at the WF terminals, and actually at all system nodes, is required to be kept above a lower limit,  $V_{min}$ , and below a high limit,  $V_{max}$ . This can be expressed as:

$$V_{min} \leq |V| \leq V_{max} \quad (28)$$

In the voltage plane, the inequality defined by (28) represents the area enclosed between two circles both centred at the origin, the inner, smaller, circle has radius  $V_{min}$  whereas the larger circle has a radius  $V_{max}$ . Minimum and maximum voltage constraints are now drawn along with the previous constraints in the voltage plane as shown in Fig. 11 with the shaded area representing the domain of allowable PQ bus voltage. It can be seen that the feasible operating area, for the present case, is limited by  $P_{Gmax}$  at the bottom, then by  $Q_{Gmin}$ , by  $V_{max}$  at the right hand side, by  $P_{Gmin}$ , line capability and  $Q_{Gmax}$  at the top, and by  $V_{min}$  on the left hand side. For a particular system the above limits may well change, and will also be influenced by changes in the operating conditions of the same system.

It is clear now that the feasible operating region of a power system node can be determined graphically in the complex voltage plane. Having the feasible operating region defined in the complex voltage plane, it can be easily mapped to the complex power plane to get the capability chart of the node at which the WF is connected. Mapping from complex voltage plane to complex power plane is done using the method described in sec. 2.2.1 and equations (22) and (23). Fig. 12 shows mapping of the constraints of fig. 11 into the complex power plane. The shaded area in Fig. 12 is the capability chart for the PQ node.

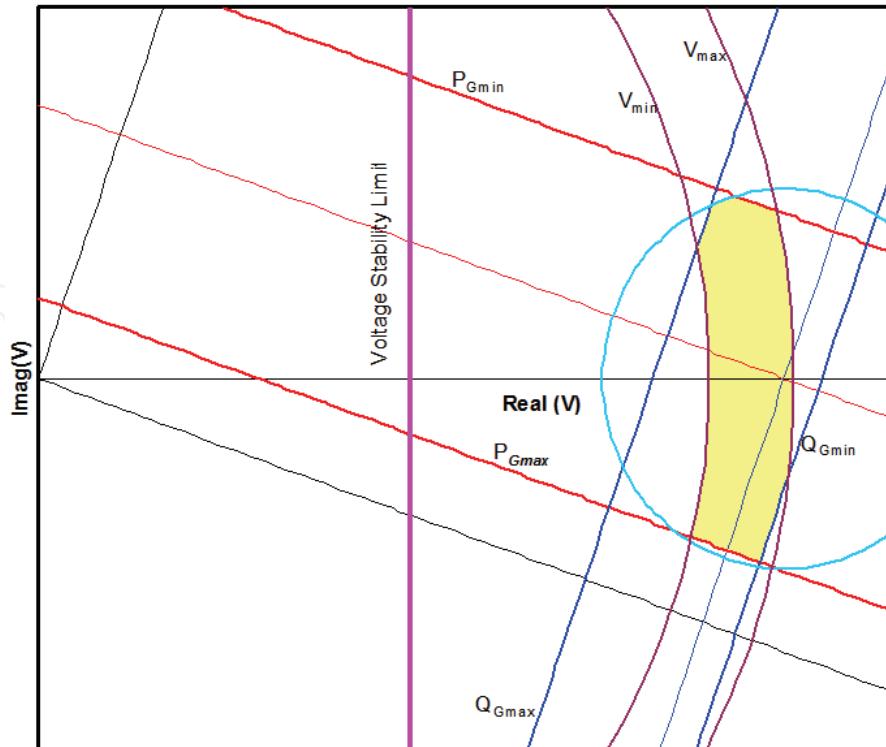


Fig. 11. The complex voltage plane with all of the constraints on the PQ node voltage

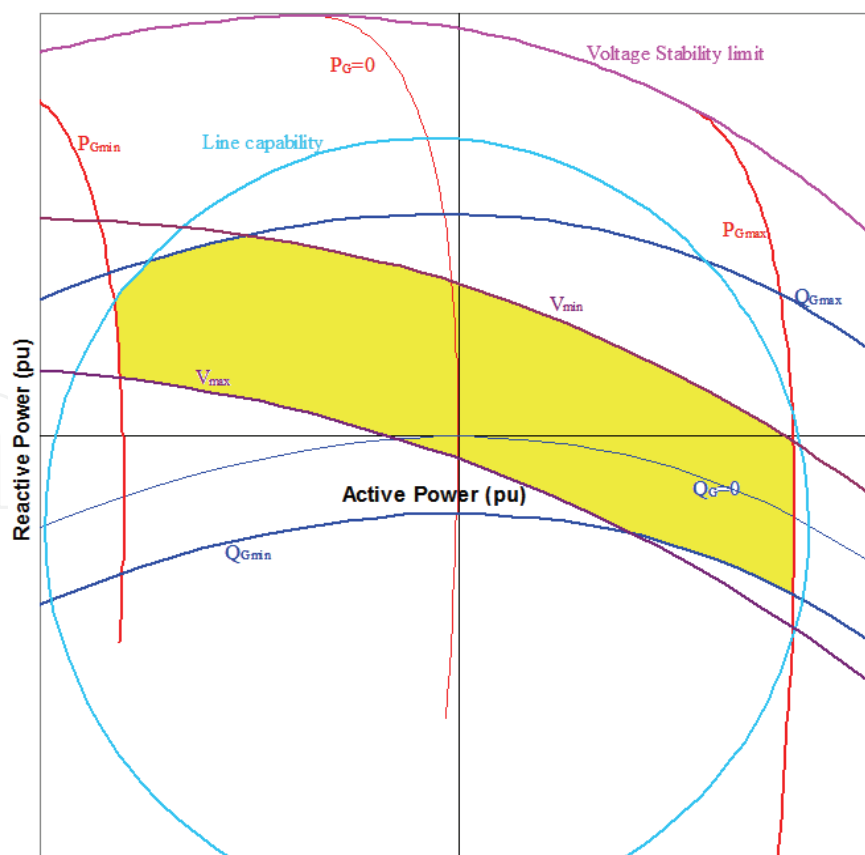


Fig. 12. Operating and stability constraints in the P-Q plane

### 3.2 Test case

IEEE 30 bus system is used as a test system for the voltage stability analysis and it will be the test system for this section as well. Bus 30 is chosen for application of the proposed method because it is the weakest bus of this system and WFs are usually connected at remote areas where the network is weak. The method can, however, be applied at any other bus. At the base case, active power load at bus 30 is 10.6 MW (0.106 pu) and the reactive power is 1.9 MVar (0.019 pu). The higher voltage solution  $V_H$ ,  $V_L$  and Thevenin equivalent are the same as in sec. 2.3. A capability chart is drawn, Fig. 13, with the load at node 30 marked by a diamond. The load point lies well within the allowable area with all the constraints satisfied.

The accuracy of the capability chart can be further tested in many different ways. A second way is to evaluate the corners of the feasible region, points A, B, C, D, E, F and G of Fig. 13. Each corner is the intersection of two constraints that are about to be violated. The active and reactive power coordinates of the corner points are used as P and Q injections at bus 30 and a detailed load flow study is carried out using DlgSILENT Power Factory software. The results are listed in Table 1, which identifies the corner points, the corresponding power injections, the limiting constraints, and the values obtained from load flow calculations for the voltage and current at bus 30. Threshold values for the constraints are shown within brackets following the first incident of each constraint. Examining the first row of the table, for corner point A, the voltage at node 30 is 1.061 pu exceeding the maximum allowable voltage; PG is -0.3326 pu which is less than  $P_{Gmin}$ ; I and QG are both within limits. The same validation can be observed for all other corner points with an error less than 2%.

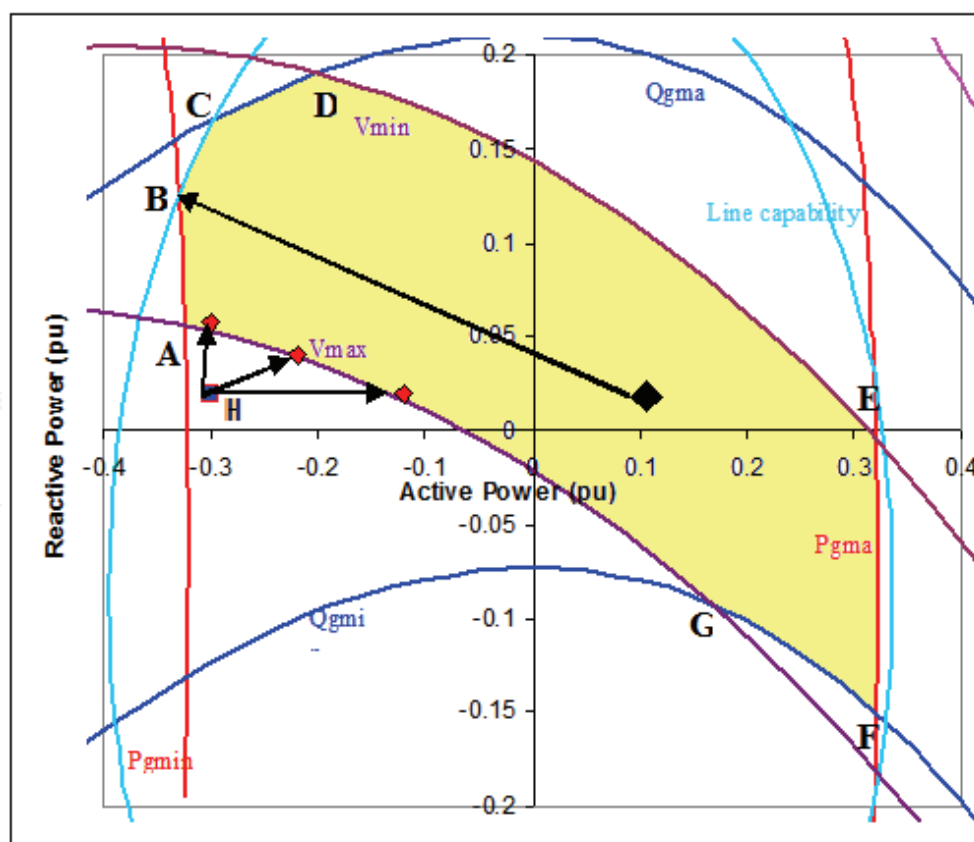


Fig. 13. The capability charts for bus 30 of the IEEE 30 bus system

As one further approach to confirm the benefits of the proposed capability chart, consider point H on Fig 13, where excessive wind generation causes an over voltage at bus 30. The three arrows emanating from H suggest three different ways to correct the situation. The first option is to maintain wind power at 30 MW and increase the reactive power consumption at bus 30 from 2 MVAR to 5.8 MVAR. A second option is to curtail 8 MW of wind power and add 2.1 MVAR load. Finally, a third option is to leave reactive power unchanged and reduce the output of the wind farm to 12 MW. These corrective actions are applied to the detailed system model, one at a time, and a load flow calculation is carried out. The voltage at bus 30 is found to be  $1.06\angle 3.85^\circ$  pu,  $1.06\angle 0.54^\circ$  pu, and  $1.06\angle -3.58^\circ$  pu for each of the three cases respectively, which is again in complete agreement with the chart.

	Power injections		Constraints Violated		Load Flow Calculated Values			
	P MW	Q MVAR			V (pu)	I (pu)	$P_G^*$ (pu)	$Q_G^*$ (pu)
A	-32.35	6.20	$V_{\max}(1.06)$	$P_{G\min}(-0.3)$	1.061	0.311	-0.3326	0.0817
B	-33	13	$I_m(0.35)$	$P_{G\min}$	1.015	0.354	-0.3402	0.1676
C	-29	17	$I_m$	$Q_{G\max}(0.25)$	0.979	0.344	-0.2989	0.2154
D	-20	19.5	$V_{\min}(0.94)$	$Q_{G\max}$	0.946	0.295	-0.2057	0.2452
E	32	-0.18	$V_{\min}$	$P_{G\max}$	0.935	0.342	0.3321	-0.0016
F	32	-14.4	$Q_{G\min}(-0.07)$	$P_{G\max}$	1.032	0.339	0.3319	-0.1276
G	16.5	-9.7	$V_{\max}(1.06)$	$Q_{G\min}$	1.061	0.180	0.1696	-0.1230

Table 1. Voltage collapse indicators for bus 30 for load shedding in different directions

#### 4. Conclusion

In this chapter, a graphical method for analysis of some network issues arising from integration of wind power at high penetration level is presented. Voltage stability for the case static power injections at a node is analysed graphically followed by analysis of the effect of a WF with large IGs connected to a system. The graphical method proved its accuracy in indicating the system state and in quick estimation of an effective remedial action.

It has been shown graphically and verified through numerical simulations that the voltage stability indicators, based on the PQ model, are not suitable for the case of a WF with IG. It has been also shown that the reactive power control of a WF does not only change quantitatively with variations in the WF output, but also qualitatively as the direction of reactive power support may be required to change. The graphical method is simple but rich in its indication and usage. Its simplicity makes it suitable for online monitoring of the WF. Also, it can be a useful educational tool helping to gain insight of WF interaction with power systems.

This chapter also presents a graphical method for determining network limits for wind power integration. For each candidate node, where a wind farm is planned, a capability

chart is constructed defining the allowable domain of power injection where all operating and security constraints are satisfied. The capability chart gives a clear indication about the allowable size of the wind farm. In case the planned wind farm size exceeds the allowable limits the chart determines the active limits and provides a quick assessment of the potential solutions.

The capability chart is fast to construct, versatile in indication, and simple to use. Therefore, it can also be a useful tool for on-line monitoring and control of power system containing wind farms or any other renewable energy resource. Relying on the information and indicators provided by the chart the operator can make decisions about local corrective actions at the node where the wind farm is connected. The accuracy of the proposed chart is validated through comparing the information obtained from the chart with those obtained from the detailed load flow calculation using the IEEE 30-bus test system, which are found to be in nearly perfect agreement with each other.

## 5. Acknowledgment

This work was supported by The Charles Parsons Energy Research Awards, which were created in September 2006 by the Minister for Communications, Marine & National Resources of Ireland and Science Foundation Ireland under the Strategy for Science, Technology and Innovation.

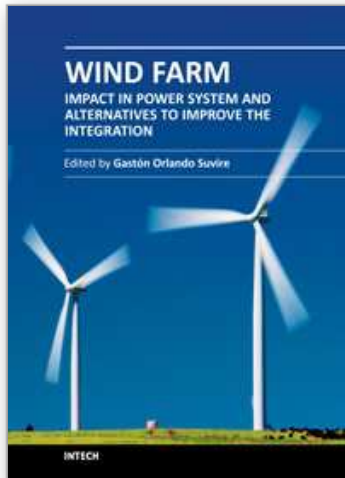
## 6. References

- Abdelkader, S.(1995). *Power system security assessments with particular reference to voltage instability*, PhD Thesis, Faculty of engineering, Mansoura University Egypt.
- Abdelkader, S.& Fox, B. (2009). Voltage Stability Assessment For Systems With Large Wind Power Generation, *Proceedings of UPEC 2009, 44th International Universities Power Engineering Conference*, pp. 14-17, ISBN 842-6508-23-3, Glasgow, Scotland, UK, September 1-4, 2009
- Abdelkader, S. & Flynn, D. (2009). Graphical determination of network limits for wind power integration. *IET Generation, transmission & Distribution*, Vol.3, No.9, (September 2009), pp. 841-849, ISSN 1751-8687
- Chebbo, A. ; Irving, M. & Sterling, M. (1992). Voltage collapse proximity indicator: behavior and implications, *IEE Generation, transmission & Distribution*, Vol.144, No.3, (May 1992), pp. 241-252, ISSN 1350-2360
- Elkateb, M.; Abdelkader, S. & Kandil, M. (1997). Linear indicator for voltage collapse in power systems. *IEE Generation, transmission & Distribution*, Vol.139, No.2, (March 1997), pp. 139-146, ISSN 1350-2360
- Kessel, P., & Glavitch, H., (1986). Estimating the voltage stability, *IEEE Trans. on Power Delivery*, Vol.1, No.3, pp. 346-354
- Semlyen. A.. Gao. B.. & Janischewskyj. W (1991). Calculation of the extreme loading condition of a power system for the assessment of voltage stability, *IEEE Trans. on Power Systems*, Vol. 6, No.1, (Jan 1991), pp. 307-312.

Tamura, Y; Mori, H. & Iwamoto, S (1983). Relationship between voltage instability and multiple load flow solutions in electric power systems, *IEEE Trans. on Power Apparatus and Systems*, Vol.PAS-102, No.3, (May 1983), pp. 1115-1123.

IntechOpen

IntechOpen



## **Wind Farm - Impact in Power System and Alternatives to Improve the Integration**

Edited by Dr. Gastón Orlando Suvire

ISBN 978-953-307-467-2

Hard cover, 330 pages

**Publisher** InTech

**Published online** 28, July, 2011

**Published in print edition** July, 2011

During the last two decades, increase in electricity demand and environmental concern resulted in fast growth of power production from renewable sources. Wind power is one of the most efficient alternatives. Due to rapid development of wind turbine technology and increasing size of wind farms, wind power plays a significant part in the power production in some countries. However, fundamental differences exist between conventional thermal, hydro, and nuclear generation and wind power, such as different generation systems and the difficulty in controlling the primary movement of a wind turbine, due to the wind and its random fluctuations. These differences are reflected in the specific interaction of wind turbines with the power system. This book addresses a wide variety of issues regarding the integration of wind farms in power systems. The book contains 14 chapters divided into three parts. The first part outlines aspects related to the impact of the wind power generation on the electric system. In the second part, alternatives to mitigate problems of the wind farm integration are presented. Finally, the third part covers issues of modeling and simulation of wind power system.

### **How to reference**

In order to correctly reference this scholarly work, feel free to copy and paste the following:

Sobhy Abdelkader (2011). Wind Power Integration: Network Issues, Wind Farm - Impact in Power System and Alternatives to Improve the Integration, Dr. Gastón Orlando Suvire (Ed.), ISBN: 978-953-307-467-2, InTech, Available from: <http://www.intechopen.com/books/wind-farm-impact-in-power-system-and-alternatives-to-improve-the-integration/wind-power-integration-network-issues>

**INTECH**  
open science | open minds

### **InTech Europe**

University Campus STeP Ri  
Slavka Krautzeka 83/A  
51000 Rijeka, Croatia  
Phone: +385 (51) 770 447  
Fax: +385 (51) 686 166  
[www.intechopen.com](http://www.intechopen.com)

### **InTech China**

Unit 405, Office Block, Hotel Equatorial Shanghai  
No.65, Yan An Road (West), Shanghai, 200040, China  
中国上海市延安西路65号上海国际贵都大饭店办公楼405单元  
Phone: +86-21-62489820  
Fax: +86-21-62489821

© 2011 The Author(s). Licensee IntechOpen. This chapter is distributed under the terms of the [Creative Commons Attribution-NonCommercial-ShareAlike-3.0 License](#), which permits use, distribution and reproduction for non-commercial purposes, provided the original is properly cited and derivative works building on this content are distributed under the same license.

IntechOpen

IntechOpen